3D modeling of IP effects on electromagnetic data in the time domain

David Marchant, Eldad Haber, Laurens Beran and Douglas W. Oldenburg, University of British Columbia*

SUMMARY

We develop a new technique for forward modeling the three-dimensional electromagnetic (EM) response of chargeable material in the time domain. The method can be applied to any type of transmitter (loop or grounded electrodes) or receiver (**H** or **E** field measurements) and operates directly in the time domain, requiring no transformations. A synthetic example of an airborne time domain survey passing above a vertical, polarizable dike is presented.

INTRODUCTION

Chargeability is considered to be one of the most diagnostic physical properties when exploring for porphyry copper deposits (Fink et al., 1990). It is typically mapped using the induced polarization (IP) technique (Seigel et al., 2007), where current is injected into the ground through a pair of transmitter electrodes and the voltage response is measured across a second pair of electrodes. Measurements can be made either in the time or frequency domain. In the time domain, the voltage decay at the receivers is recorded after the transmitter current is interrupted. In the frequency domain, a sinusoidally varying current is injected at different frequencies, and the change in voltage and/or phase shift is recorded.

Conventional IP, however, is not the only EM method that is sensitive to chargeable material. Any electromagnetic measurement taken in the presence of a chargeable material will be affected. Unfortunately, the effects are often hard to recognize in the data. For the particular case of coincident loop time-domain EM data, negative transients - soundings with a reversal in sign of the received field - are diagnostic of chargeable material. While early papers speculated that this effect could be caused by particular conductivity distributions or magnetic effects, Weidelt (1982) showed that for a coincident loop system with a step-off primary field, the measured secondary field must be non-negative over non-polarizable ground, regardless of the subsurface distribution of conductivity. Observed negative transients in coincident loop EM systems can therefore only be attributed to polarization effects; that is, the conductivity of the ground is time-varying.

Negative transients are commonly observed in airborne TEM systems, such as AeroTEM or VTEM. An example, taken from a VTEM survey performed over the Mt. Milligan deposit in British Columbia is shown in Figure 1. However, negative transients in these multi-static TEM systems are not necessarily indicative of polarization effects (Smith, 1988). For example, a non-polarizable earth can produce polarity reversals in the measured data when receivers are placed outside of the transmitter. Furthermore, the proof in Weidelt (1982) requires some conditions on the transmitting waveform that are not always fulfilled in practice.

This ambiguity has motivated a number of modeling studies which seek to determine features of TEM data that can be used to identify polarization effects. The majority of these compute the EM response in the frequency domain and then transform those results back to the time domain (Flis et al. (1989), Beran and Oldenburg (2008)). In order to achieve an accurate solution in the time domain over large time intervals, these techniques must solve the frequency domain forward problem at a large number of frequencies, spanning many decades. This is not a problem when considering simple 1D layered earth models, but it can be prohibitively difficult when considering large three dimensional problems.

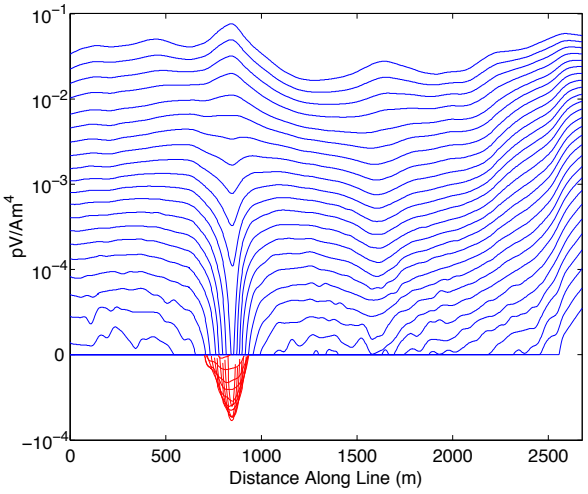

(a)

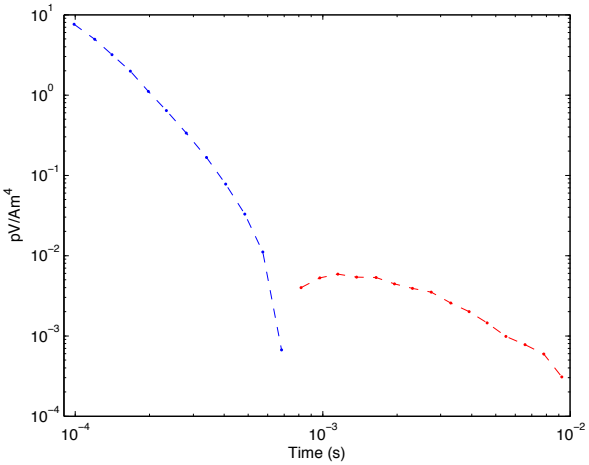

(b)

Figure 1: Example of a negative transient observed in a VTEM survey at the Mt. Milligan deposit in British Columbia (a) Line of data above the deposit. (b) Single sounding at 850m along the line. Data in red are negative.

SEG Las Vegas 2012 Annual Meeting

DOI http://dx.doi.org/10.1190/segam2012-1454.1

In order to further understand how polarizability effects are manifested in TEM data for an arbitrary system, we have developed a three-dimensional time domain forward modeling code that directly incorporates polarizability effects via a space-time-varying conductivity. The method uses an implicit discretization in time and requires no numerical transformations from the frequency domain. We can model any type of transmitter (loop or grounded electrodes) and can calculate the response of either the magnetic or electric fields. Here we first introduce the Cole-Cole model, which parameterizes the conductivity in the frequency domain. We then derive a finite volume discretization of Maxwell's equations, with the Cole-Cole model now represented in the time-domain as a coupled ordinary differential equation. The technique is demonstrated on a synthetic example that exhibits negative transients in airborne time domain data.

DISPERSION MODELS

The presence of chargeable material indicates that the conductivity of the ground varies with time or frequency. The frequency dependence of a material is often parameterized by the Cole-Cole model (Pelton et al., 1978)

$$\rho(\omega) = \rho_0\left(1-\eta\left(1-\frac{1}{1+(i\omega\tau)^c}\right)\right) \tag{1}$$

In this expression, ρ_0 is the resistivity (Ωm) at zero frequency, η is the chargeability, τ is a time constant (seconds), and c is the frequency dependence. The chargeability has a value between 0 and 1. It determines the magnitude of the difference in the resistivity between the low and high frequency asymptotes. The value of the time constant determines the frequency at which the magnitude of the imaginary resistivity peaks. The frequency dependence controls the sharpness of the transition between the two asymptotic values. In the special case where $c = 1$, the model simplifies to the Debye model, and the transition occurs rapidly. It has been suggested that c = 0.5 best represents the type of the dispersion curve observed in disseminated mineralization (Wong, 1979). This results in broader a dispersion curve, with a slower transition between the two asymptotic values (Figure 2).

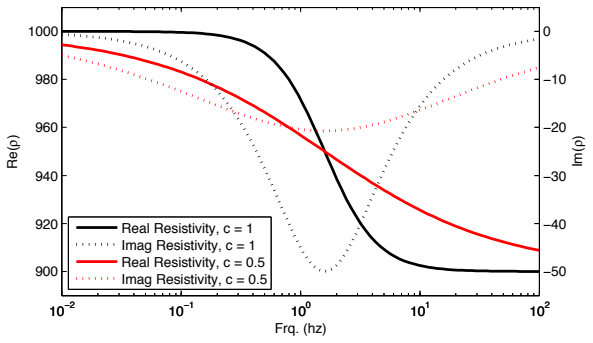

Figure 2: Cole-Cole Models for c=1 and c=0.5

Another way to parameterize the dispersion of a chargeable material is to express the the frequency dependent resistivity as a superposition of a spectrum of Debye models, each with a different η and τ (Morgan and Lesmes (1994), Nordsiek and Weller (2008)). This model can be written as

$$\rho(\omega) = \rho_0\left(1-\sum_{k=1}^{n}\eta_k\left(1-\frac{1}{1+i\omega\tau_k}\right)\right) \tag{2}$$

If enough terms are used this model can fit any Cole-Cole dispersion curve. It can also fit dispersion curves exhibiting more than one peak, as observed in (Pelton et al., 1978).

THEORY

Maxwell's equations in the frequency domain are

$$\nabla\times\mathbf{E}+i\omega\mu\mathbf{H}=0 \tag{3a}$$
$$\nabla\times\mathbf{H}-\mathbf{J}=\mathbf{s} \tag{3b}$$
$$\mathbf{E}(\omega)=\rho(\omega)\mathbf{J}(\omega) \tag{3c}$$

Where $\mathbf{H}$ is the magnetic field, $\mathbf{E}$ is the electric field and $\mathbf{J}$ is the volume current density. $\rho(\omega)$ is the frequency dependant resistivity distribution and μ is the magnetic permeability. $\mathbf{s}$ is a source term, which can consist of either inductive (wire loop) or galvanic (grounded electrodes) sources.

We will first consider only resistivity distributions that exhibits Debye dispersions. Ohm's law (3c) becomes

$$\mathbf{E}=\rho_0\left(1-\eta\left(1-\frac{1}{1-i\omega\tau}\right)\right)\mathbf{J} \tag{4a}$$
$$=\rho_0\frac{1+i\omega\tau-i\omega\tau\eta}{1+i\omega\tau}\mathbf{J} \tag{4b}$$

Or

$$\sigma_0\mathbf{E}+i\omega\tau\sigma_0\mathbf{E}=\mathbf{J}+i\omega\tau(1-\eta)\mathbf{J} \tag{5}$$

Where σ_0 is equal to the conductivity observed at zero frequency, $\sigma_0=\frac{1}{\rho_0}$. Equations 3a, 3b and 5 can now be transformed to the time domain giving

$$\nabla\times\mathbf{e}+\mu\mathbf{h}_t=0 \tag{6a}$$
$$\nabla\times\mathbf{h}-\mathbf{j}=\mathbf{s} \tag{6b}$$
$$\sigma_0\mathbf{e}+\tau\sigma_0\frac{\partial\mathbf{e}}{\partial t}=\mathbf{j}+\tau(1-\eta)\frac{\partial\mathbf{j}}{\partial t} \tag{6c}$$

By discretizing in time using the backward Euler method with a step size $k=\delta t^{-1}$ we obtain

$$\nabla\times\mathbf{e}_{n+1}+\mu k(\mathbf{h}_{n+1}-\mathbf{h}_n)=0 \tag{7a}$$
$$\nabla\times\mathbf{h}_{n+1}-\mathbf{j}_{n+1}=\mathbf{s}_{n+1} \tag{7b}$$
$$\sigma_0\mathbf{e}_{n+1}+k\tau\sigma_0(\mathbf{e}_{n+1}-\mathbf{e}_n)=\mathbf{j}_{n+1}+k\tau\gamma(\mathbf{j}_{n+1}-\mathbf{j}_n) \tag{7c}$$

Where $\gamma=1-\eta$. $\mathbf{e}_{n+1}$ and $\mathbf{j}_{n+1}$ can be eliminated from the system leaving a single equation only in terms of $\mathbf{h}_{n+1}$

$$\nabla\times\tilde{\rho}\nabla\times\mathbf{h}_{n+1}+\mu k\mathbf{h}_{n+1}=\mu k\mathbf{h}_n+\nabla\times\left(\tilde{\rho}\mathbf{s}_{n+1}+\tilde{a}\mathbf{j}_n-\tilde{b}\mathbf{e}_n\right) \tag{8}$$

DOI http://dx.doi.org/10.1190/segam2012-1454.1

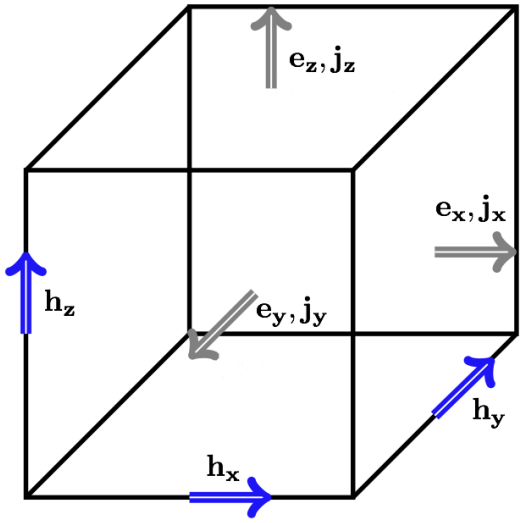

Figure 3: Staggered discretization in 3D. Physical properties are defined at cell centres.

Where we have defined the new parameters

$$\tilde{\rho} = \frac{1+k\tau\gamma}{\sigma_0\,(1+k\tau)} \tag{9}$$

$$\tilde{a} = \frac{k\tau\gamma}{\sigma_0\,(1+k\tau)} \tag{10}$$

$$\tilde{b} = \frac{k\tau}{(1+k\tau)} \tag{11}$$

For numerical evaluation, we discretize the system on an orthogonal, staggered grid and use a finite volume approach (Yee, 1966) with material averaging of properties (Haber and Ascher, 2001). We place all physical properties at the centre of cells, **h** on cell edges and **e** and **j** on cell faces (Figure 3). The discrete equation is

$$\left(\mathbf{curl}\,\mathrm{diag}\left(\mathbf{A_c^f}\tilde{\rho}\right)\mathbf{curl}^\top + \mathbf{grad}\,\mathrm{diag}\left(\mathbf{A_c^n}\tilde{\rho}\right)\mathbf{grad}^\top + \mu k\right)\mathbf{h}_{n+1} = \mathbf{curl}\left(\mathrm{diag}\left(\mathbf{A_c^f}\tilde{\rho}\right)\mathbf{s}_{n+1} + \mathrm{diag}\left(\mathbf{A_c^f}\tilde{a}\right)\mathbf{j}_n - \mathrm{diag}\left(\mathbf{A_c^f}\tilde{b}\right)\mathbf{e}_n\right) \tag{12}$$

Where **curl** and **grad** are the discrete form of the curl and gradient operators obtained by short differences on staggered grids and $\mathbf{A_c^f}$ and $\mathbf{A_c^n}$ are averaging matrices from cell centres to faces and nodes respectively. The system is solved by a direct solver (MUMPS) (Amestoy et al., 2006).

Given the initial state of the fields $\mathbf{h}_0$, $\mathbf{e}_0$ and $\mathbf{j}_0$, the source term $\mathbf{s}_n$ and the distribution of the physical properties σ_0, η, and τ, Equation 12 can be solved for $\mathbf{h}_{n+1}$. $\mathbf{e}_{n+1}$ and $\mathbf{j}_{n+1}$ can then be calculated using

$$\mathbf{j}_{n+1} = \mathbf{curl}\,\mathbf{h}_{n+1} - \mathbf{s}_{n+1} \tag{13}$$

$$\mathbf{e}_{n+1} = \tilde{\rho}\mathbf{j}_{n+1} - \tilde{a}\mathbf{j}_n + \tilde{b}\mathbf{e}_n \tag{14}$$

This process is then repeated for each time step.

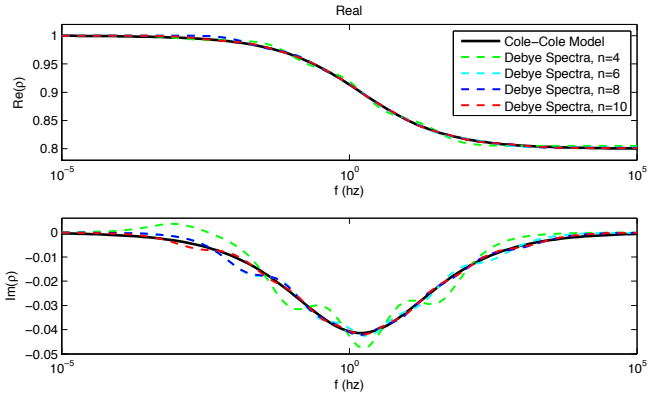

Figure 4: Comparison of a Cole-Cole dispersion (solid black line) with a superimposed Debye spectra (Equation 2) of varying n. A good fit can be achieved with relatively few terms.

Non-Debye dispersion spectra

It is easy to show that dispersion spectra of the form or Equation 2 can be written as a Padé approximation of the form

$$\rho\,(\omega) = \rho_0 \frac{\sum_{k=0}^{n}(i\omega)^k p_k}{1+\sum_{k=1}^{n}(i\omega)^k q_k} \tag{15}$$

Where p and q are parameters that depend on η_i and τ_i. Substituting this dispersion spectra into Ohm's law (Equation 3c) gives

$$\sigma_0\mathbf{E} + \sigma_0\sum_{k=1}^{n}(i\omega)^k q_k\mathbf{E} = \mathbf{J} + \sum_{k=1}^{n}(i\omega)^k p_k\mathbf{J} \tag{16}$$

Transforming to the time domain yields

$$\sigma_0\mathbf{e} + \sigma_0\sum_{k=1}^{n} q_k\frac{\partial^k}{\partial t^k}\mathbf{e} = \mathbf{j} + \sum_{k=1}^{n} p_k\frac{\partial^k}{\partial t^k}\mathbf{j} \tag{17}$$

Increasing the number of terms in the above summation allows for a greater variety of dispersion curves to be represented accurately, but comes with the cost of increasing the order of the ODE in Equation 17. If a backward Euler method is used to discretize in time, the inclusion of these higher order terms requires that the values of **e** and **j** at previous time steps be stored. This increases the memory requirements of the forward modeling, but not prohibitively so as long as the n is relatively small.

EXAMPLE

In order to test the technique, the time domain response of an airborne EM survey passing above a vertical polarizeable dike (Figure 6(a)) was modelled. The dike had a zero-frequency resistivity (ρ_0) of $10\Omega m$, a time constant (τ) of $0.01s$, a chargeability (η) of 0.1 and a frequency dependence (c) of 1. The dike had infinite depth and North-South extent and was placed in a $100\Omega m$ half-space.

The model was discretized onto a 70 by 50 by 50 cell mesh. The core region (40 by 20 by 20) had a cell size of 25m. 15

DOI http://dx.doi.org/10.1190/segam2012-1454.1

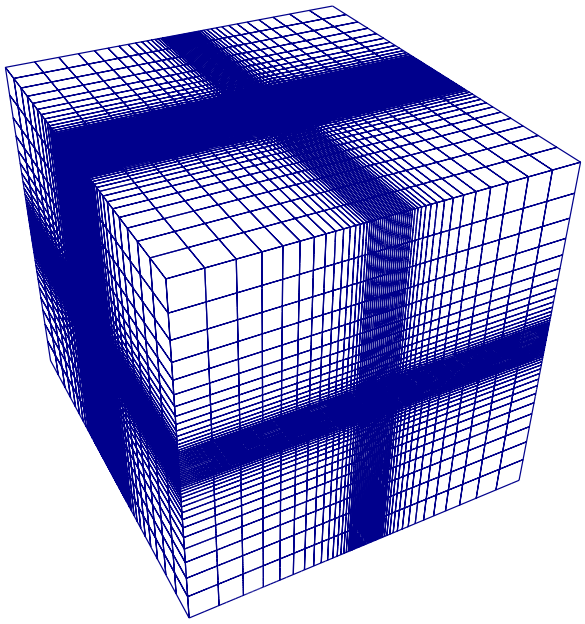

Figure 5: Mesh for synthetic example. Core cells are 25m on a side, and the mesh contains 187,500 cells.

padding cells were added to each side of the mesh expanding with a constant expansion ratio of 1.2 (Figure 5).

A single line consisting of 30 transmitter-receiver pairs was modelled. The transmitter consisted of a horizontal loop with a radius of 10m, flying 30m above the earth's surface. The receivers were placed at the centre of each of the transmitter loops. The transmitter waveform was modelled to be a perfect step off, and measurements of the vertical component of $\frac{dB}{dt}$ were taken starting at 10^{-4} seconds and extended to 10^{-2} seconds.

The resulting data are shown in Figures 6(b) and 6(c). A negative transient is clearly apparent in the data with a zero crossing occurring at approximately 10^{-3} seconds.

CONCLUSIONS

We have developed a technique to forward model the EM response of a chargeable body directly in the time domain. The technique can model any type of transmitter (loop or grounded electrodes) and can calculate the response of either the magnetic or electric fields. The technique was initially developed for models exhibiting Debye dispersion and then extended to be able to model the response from dispersions of the form of Equation 2. The method was tested on a synthetic example of a chargeable dike in a uniform half-space. Negative transients were observed in modelled airborne time-domain measurements above the polarizable body.

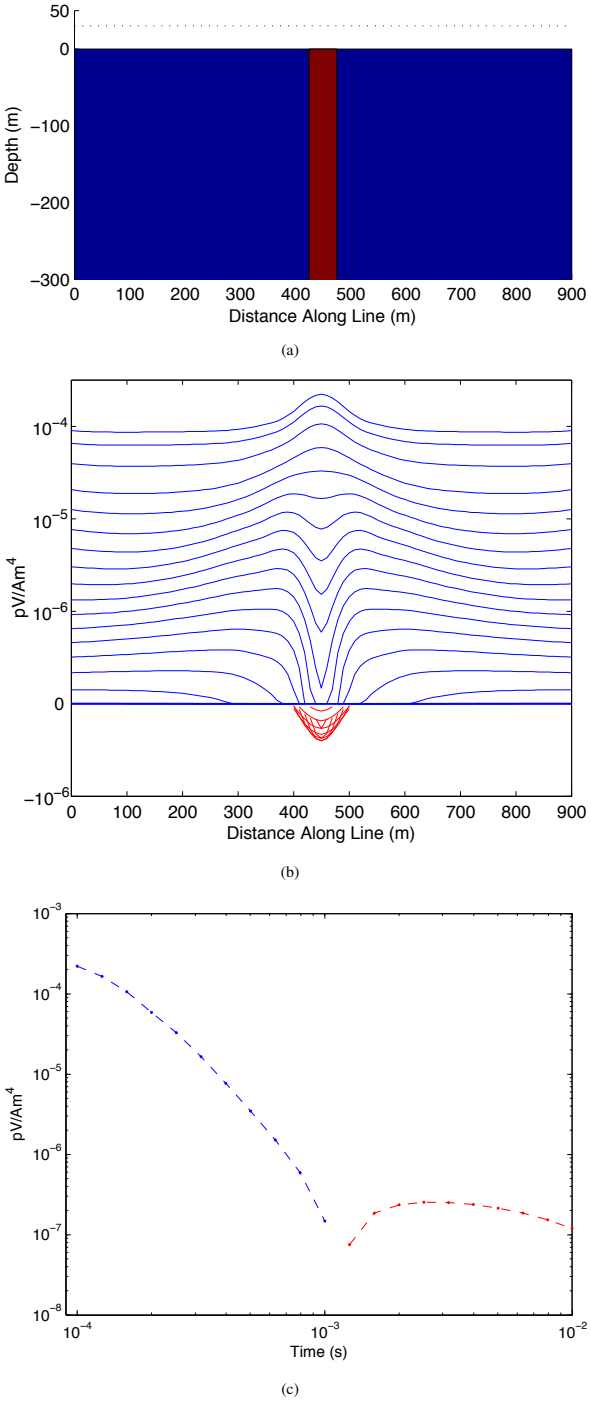

Figure 6: (a) A cross-section through the synthetic model. The vertical dike is chargeable. (b) Line profiles of the data. An obvious zero crossing occurs in the late time channels as the receiver passes over the dike. (c) Decay curve observed directly over the chargeable dike. A zero crossing occurs at approximately 10^{-3} seconds. Data in red are negative.

DOI http://dx.doi.org/10.1190/segam2012-1454.1

http://dx.doi.org/10.1190/segam2012-1454.1

EDITED REFERENCES

Note: This reference list is a copy-edited version of the reference list submitted by the author. Reference lists for the 2012 SEG Technical Program Expanded Abstracts have been copy edited so that references provided with the online metadata for each paper will achieve a high degree of linking to cited sources that appear on the Web.

REFERENCES

Amestoy, P. R., A. Guermouche, J. Y. L'Excellent, and S. Pralet, 2006, Hybrid scheduling for the parallel solution of linear systems: Parallel Computing, **32**, 136–156.

Beran, L., and D. Oldenburg, 2008, Estimation of Cole-Cole parameters from time-domain electromagnetic data: 78th Annual International Meeting, SEG, Expanded Abstracts, 569–573.

Fink, J. B., ed., 1990, Induced polarization: Applications and case histories: SEG.

Flis, M. F., G. A. Newman, and G. W. Hohmann, 1989, Induced-polarization effects in time-domain electromagnetic measurements: Geophysics, **54**, 514–523.

Haber, E., and U. M. Ascher, 2001, Fast finite volume simulation of 3D electromagnetic problems with highly discontinuous coefficients: SIAM Journal on Scientific Computing, **22**, 1943–1961.

Morgan, F. D., and D. P. Lesmes, 1994, Inversion for dielectric relaxation spectra: The Journal of Chemical Physics, **100**, 671–681.

Nordsiek, S., and A. Weller, 2008, A new approach to fitting induced-polarization spectra: Geophysics, **73**, no. 6, F235–F245.

Pelton, W. H., S. H. Ward, P. G. Hallof, W. R. Sill, and P. H. Nelson, 1978, Mineral discrimination and removal of inductive coupling with multifrequency IP: Geophysics, **43**, 588–609.

Seigel, H., M. Nabighian, D. S. Parasnis, and K. Vozoff, 2007, The early history of the induced polarization method: The Leading Edge, **26**, 312–321.

Amith, R. S., 1988, A plausible mechanism for generating negative coincident-loop transient electromagnetic responses: Ph.D. dissertation, University of Toronto.

Weidelt, P., 1982, Response characteristics of coincident loop transient electromagnetic systems: Geophysics, **47**, 1325–1330.

Wong, J., 1979, An electrochemical model of the induced polarization phenomenon in disseminated sulfide ores: Geophysics, **44**, 1245–1265.

Yee, K. S., 1966, Numerical solution of initial boundary value problems involving Maxwell's equations in isotropic media: IEEE Transactions on Antennas and Propagation, **14**, no. 3, 302–307.